Review

The Interconnection Between 3D and 4D Printing and Rheology: From Extrusion and Nozzle Deposition to Final Product Functionality

Thomas Goudoulas and Theodoros Varzakas *

Posted Date: 10 March 2026

doi: 10.20944/preprints202603.0723.v1

Keywords: 3D food printing; 4D printing; rheology; edible inks; network architecture; post-printing treatment; stimuli-responsive materials; extrusion-based printing

 doi:10.20944/preprints202603.0723.v1

Review

The Interconnection Between 3D and 4D Printing and Rheology: From Extrusion and Nozzle Deposition to Final Product Functionality

Thomas Goudoulas [1] and Theodoros Varzakas [2,*]

[1] TUM School of Life Sciences, Lehrstuhl für Brau- und Getränketechnologie, 85354 Freising, Germany

[2] Department of Food Science and Technology, University of the Peloponnese, Antikalamos, 24100 Kalamata, Greece

* Correspondence: t.varzakas@uop.gr; Tel.: +302721045279

Abstract

The successful application of 3D and 4D food printing is fundamentally governed by the rheology and microstructure of edible inks. These factors control every step, from extrusion and nozzle deposition to the final product functionality. This review systematically examines how formulation variables, including starch/protein composition, water content, and hydrocolloids, determine the network architecture and critical rheological properties, such as yield stress and viscoelasticity. These properties determine printing outcomes such as filament formation, stacking accuracy, and the stability of sensitive components. This review explores 4D printing as a "3D + 1D function," where printed structures provide additional features over time, such as a controlled color change or bioactive release, while post-printing treatment often activates these features. Through case studies of novel inks, we show how interfacial chemistry and process parameters influence texture and stability. Finally, we discuss the application of rheological metrics for predicting printability and outline the critical need for developing multi-parameter, process-relevant printability indices to advance the field of digital food manufacturing.

Keywords: 3D food printing; 4D printing; rheology; edible inks; network architecture; post-printing treatment; stimuli-responsive materials; extrusion-based printing

1. Introduction

Three-dimensional (3D) food printing has transitioned from an exploratory fabrication method to a digitally controlled manufacturing strategy capable of tailoring geometry, texture, porosity, and nutritional composition with high spatial precision. However, the feasibility of extrusion-based food printing is governed less by hardware sophistication than by the physicochemical behavior of edible inks under flow and after deposition. Recent critical syntheses emphasize that printability emerges from a delicate balance between shear-induced fluidization inside the nozzle and rapid structural recovery once the material is deposited [1,2]. Thus, rheology—rather than composition alone—acts as the central determinant linking formulation to structural fidelity.

The extension toward four-dimensional (4D) food printing further elevates the importance of this coupling. By introducing time as a functional dimension, 4D systems enable printed structures to undergo programmed transformations triggered by thermal, pH, enzymatic, hydration, or other environmental stimuli. In such systems, the rheological and microstructural characteristics that ensure successful filament formation and stacking must also support controlled post-printing evolution [3]. Consequently, 4D food printing can be conceptualized as "3D structure plus temporally activated functionality," where network architecture dictates not only geometric stability but also transformation kinetics and diffusion-driven processes [4].

 doi:10.20944/preprints202603.0723.v1

Across recent literature, three tightly interconnected elements repeatedly emerge as governing factors: network architecture, critical rheological parameters, and process mechanics. Gel-based edible inks—particularly starch–hydrocolloid and protein–polysaccharide composites—have been systematically mapped in terms of composition–rheology–geometry relationships, revealing that yield stress, storage modulus, and thixotropic recovery define operational printability windows [1,5,6]. Composite starch systems reinforced with carrageenan or alginate demonstrate how modest compositional shifts can shift inks from spreading-dominant to self-supporting regimes [7,8]. Similarly, plant-protein-based matrices and alternative protein systems illustrate how mechanical strength and infill architecture can be engineered to replicate conventional food textures while maintaining extrusion stability [9,10].

Yet viscosity alone is insufficient to predict performance. Experimental and modeling studies increasingly converge on the role of yield stress, viscoelastic balance (G′/G″), and recovery kinetics as primary determinants of filament integrity and multi-layer stacking accuracy [11,12]. Advanced analyses further propose dimensionless frameworks linking elastoviscoplastic behavior to die swelling, spreading, and deposition regimes, suggesting that predictive printability indices must integrate rheological and process variables rather than treating them independently [13]. Computational fluid dynamics (CFD) modeling reinforces this integration by demonstrating how shear-rate distributions and pressure gradients within the nozzle geometry directly translate into structural outcomes after extrusion [14].

Beyond geometric fidelity, the functional performance of printed foods increasingly depends on internal architecture and interfacial engineering. Emulsion-based systems and coaxial extrusion strategies enable encapsulation and protection of sensitive bioactives, significantly enhancing storage stability and bioaccessibility relative to non-structured formulations [15,16]. 3D printing of dairy products benefits from physical, chemical, or enzymatic modification and additive incorporation, improving printability and nutrition. Hydrophilic gels, calcium, and lipids enhance gel properties and structural fidelity [17]. Cellulose-based inks, especially with carboxymethyl cellulose, offer shear-thinning and thermal stability, particularly at low concentration, supporting custom nutritionally controlled foods for future applications [18]. Likewise, gel-in-gel constructs for probiotic delivery demonstrate that controlled rheology not only preserves structural precision but also improves microbial survival and release kinetics during digestion [19]. These findings illustrate a critical conceptual shift: the same rheological descriptors that govern extrusion also regulate mass transfer, degradation, and stimuli-responsive behavior in the final product.

Despite rapid progress, the literature remains partially fragmented. Foundational reviews address edible ink categories and rheological fundamentals [20–22], while emerging perspectives focus on intelligent systems integrating monitoring and control [4,23,24], or functional and bioactive-enriched formulations that develop low glycemic index food inks for diabetic patients through in vivo studies [25]. However, a unified framework that systematically connects ingredient-level network formation, quantitative rheological metrics, extrusion mechanics, structural fidelity, and post-printing functionality is still evolving. Without such integration, formulation development remains largely empirical, limiting scalability and reproducibility.

This review synthesizes advances from 2020 onward to articulate a coherent continuum of materials–rheology–process–function for 3D and 4D food printing. Our goal is to provide guidelines for testing the performance of various inks and printed food matrices rather than conducting an extensive descriptive technological analysis. By positioning rheology as the mechanistic bridge between formulation and final product performance, we aim to consolidate current knowledge into a structured perspective that supports rational ink design, predictive printability assessment, and the development of multi-parameter indices suitable for next-generation digital food manufacturing.

 doi:10.20944/preprints202603.0723.v1

2. Network Architecture in Edible Ink Formulations

2.1. Gel Network Formation and Molecular Architecture

The success of 3D food printing depends on the formation and stability of gel networks that reconcile two competing physical requirements: low resistance to flow under nozzle shear stress during extrusion, and rapid recovery of elastic structure after deposition to preserve geometric integrity. Qin et al. [1] established the critical foundation for understanding how formulation variables determine network architecture, defining edible hydrogels as the central material class reconciling these needs through hydrogel formulations spanning gelatin, alginate, pectin, carrageenan, agar, starch-based gels, and protein-polysaccharide composites.

Network architecture is determined by primary stabilization mechanisms that fall into distinct categories: ionic crosslinking (exemplified by *β*-carrageenan systems achieving storage moduli >4000 Pa through K^+ coordination [26], physical-ionic hybrids (gelatin-alginate systems with moderate density, G' ~2500 Pa through Ca^{2+} bridging [27], hydrogen-bonded polysaccharide blends (xanthan-locust bean gum achieving G' ~2800 Pa through van der Waals forces), and dual-crosslinked protein-polysaccharide systems (gelatin-Type B and k-carrageenan) achieving superior G' ~5000 Pa through combined ionic and covalent interactions [28]. The delicate balance between attractive and repulsive forces facilitates effective self-assembly, while excessive intermolecular forces result in functional instability and phase separation.

The molecular assembly process in gelatin-based systems differs fundamentally from starch-based networks. Oyinloye & Yoon [29] demonstrated that oil incorporation (both saturated coconut oil and unsaturated soybean oil) modulates the gelatin network structure dramatically: coconut oil at 1–3 g/100g increases density via protein-lipid interactions, while soybean oil above 5 g/100g causes phase separation and porosity. Network density quantitatively relates to microstructural features observable through scanning electron microscopy (SEM) and Fourier-transform infrared spectroscopy (FTIR), with Ahmad et al. [14] demonstrating that FTIR analysis reveals gel strengthening primarily driven by non-covalent interactions, hydrogen bonding, and electrostatic effects.

2.2. Composition-Dependent Network Properties

Starch concentration exerts critical control over network formation. Rodríguez-Herrera et al. [11] established that nixtamalized corn flour content in the range of 30-32.5 wt% optimizes both extrudability and self-supporting structural recovery, with concentrations below 30% resulting in excessive material spreading and flattening, while concentrations exceeding 32.5% reduce extrudability significantly. The optimal range reflects the balance point where starch gelatinization (occurring at ~71.8±0.2°C for arrowroot starch creates sufficient network crosslinking without compromising flow properties under extrusion pressure [12].

Water content functions as the primary gelation trigger, with research establishing that 65-80 wt% water represents the critical range for stable gel formation. Deviations below 60% result in incomplete gelation and reduced network strength, while water contents exceeding 85% reduce printability due to over-hydration, weakening intermolecular bonding. Dushina et al. [30] quantitatively demonstrated this principle: lupine callus tissue inks with 80 g/100mL callus (CT80) exhibited significantly reduced viscosity (5.6 kPa·s at 20°C versus 75.4 kPa·s for control CT0 samples) and storage modulus values 7.9 times lower than controls, with fracture stress reduced from 13,241±2329 Pa to 1621±711 Pa.

Hydrocolloid selection determines the nature of gel network formation. Nikolaou et al. [26] demonstrated that β-carrageenan-reinforced starch gels consistently achieve superior viscoelastic behavior (G' > 4000 Pa), optimal tan δ values (0.096-0.169), and yield stress conducive to stable extrusion (up to 350 Pa in gelatin-*β*-carrageenan systems), achieving 93-96% structural fidelity with <4% dimensional deviation. Bai et al. [31] showed that konjac glucomannan and curdlan blends synergistically enhance gel properties: konjac glucomannan concentration at 2.25% combined with

 doi:10.20944/preprints202603.0723.v1

curdlan at 0.75% (KGM/CD ratio 3:1) achieved optimal printing accuracy of 4.97±0.45% with superior flow behavior index (n = 0.049±0.014), indicating enhanced flowability.

The synthesized network architecture data demonstrates that dual-crosslinked systems (gelatin-*β*-carrageenan) achieve G' ~5000 Pa with tan δ ~0.18, while starch-protein systems exhibit lower G' (~1500 Pa) but offer distinct mechanical advantages through protein aggregation mechanisms. Kaliampakou et al. [27] employed principal component analysis and Taguchi's Design of Experiments, showing that viscosity, tan δ, G', and G'' collectively govern blend behavior, with 85% pore area printability achieved through optimized parameter settings.

2.3. Microstructural Characterization and Spatial Organization

Network structure exhibits hierarchical organization across multiple length scales. Oliveira et al. [32] developed phase-separated edible inks through segregative phase separation using gellan gum matrix structured with whey protein isolate beads ranging from below 5 μm to over 100 μm in diameter, demonstrating that controlled microstructure enables high-speed printing (>25-50 mm/s) at low forces (<50 N) and stresses (<500 Pa). The key insight emerged that reducing bead size and length increases viscosity, enhancing the dimensional accuracy of printed structures.

Low-field nuclear magnetic resonance (LFNMR) analysis provides a quantitative assessment of water distribution and network rigidity. Li et al. [28] combined FTIR, XRD, LFNMR, and SEM to demonstrate that hybrid binary systems (gelatin-Type B with k-carrageenan) with optimized ratios produce reduced free water content relative to bound water, indicating tighter network cross-linking and superior structural recovery post-printing.

Network mechanical properties assessed through texture analysis directly correlate with printability outcomes. Liu et al. [33] comprehensively characterized cereal-legume starch-based gels formulated with germinated brown rice and red adzuki bean flours, achieving hardness values of 1066.74±102.09 N for the RG2:1 formulation (red adzuki bean:germinated brown rice = 2:1) with printing accuracy of 99.37±0.39%, demonstrating that optimal hardness ranges and springiness values (0.64±0.10) translate directly to superior 3D printing fidelity.

3. Critical Rheological Properties Governing Printability

3.1. Yield Stress and Extrusion Stability

The success of extrusion-based printing depends critically on optimizing the rheological envelope by tuning the critical rheological properties. Kadival et al. [22] demonstrate that yield stress, storage modulus, and apparent viscosity must be simultaneously tuned to enable stable extrusion while maintaining structural fidelity post-deposition, with optimal values achieved through both formulation design and pre-processing modifications. Yield stress (σy), the minimum stress required to initiate material flow, represents one of the most critical parameters determining whether extrusion-based printing succeeds or fails. Rodríguez-Herrera et al. [11] established that stable printability for nixtamalized corn doughs occurs within specific yield stress ranges, demonstrating the fundamental principle that σy <100 Pa results in excessive spreading and material collapse, while σy >500 Pa causes extrusion difficulties and potential nozzle blockage. The optimal operating window spans 100-500 Pa, with σy ~250 Pa providing a balance between extrudability and structural retention.

Novel ink materials and emerging applications continuously enforce the rheological investigation. Recently, Choudhury et al. [34] demonstrated skim milk (SM) powder to peanut-based chenna inks, achieving direct ink writing through cold extrusion with yield stress, loss/storage modulus optimization at 2:1 composition of SM:peanut chenna with optimal processing parameters. Agarwal et al. [35] quantitatively assessed yield stress variation across psyllium husk (PH)-gelatin (G) blends: the 50PH+50G formulation (optimal for 3D printing) exhibited 109.16±9.85 Pa yield stress, the 75PH+25G formulation σy = 268.74±13.56 Pa, and the 100PH reference σy = 18.59±4.21 Pa. These data demonstrated that formulation composition enables precise yield stress tuning, with the selected 50PH+50G blend achieving the highest mechanical strength (Young's modulus 9.17±0.088 kPa)

 doi:10.20944/preprints202603.0723.v1

among tested ratios despite having lower yield stress than the 75PH+25G alternative, indicating complex relationships between yield stress and other mechanical properties.

3.2. Viscoelasticity and the Storage-Loss Moduli Balance

The viscoelastic balance between elastic (storage modulus G') and viscous (loss modulus G") behavior fundamentally determines whether printed structures maintain geometric fidelity or collapse post-deposition. Herrada-Manchón et al. [2] established that essential hydrogel rheology characterization requires measurement of yield stress, shear-thinning behavior, thixotropy, viscoelasticity, and gelling mechanisms, emphasizing that understanding these characteristics is essential for optimizing extrusion-based 3D printing. The critical principle emerges that optimal 3D printing inks require G' >> G" (storage modulus dominance) to provide structural integrity, while G' >> σy ensures self-supporting capability without excessive spreading. Nikolaou et al. [26] demonstrated that β-carrageenan-starch composites consistently achieve storage moduli >4000 Pa—establishing this as a practical threshold for gel-like behavior and structural self-support. For comparison, Kaliampakou et al. [27] showed that gelatin-alginate systems achieve G' ~2500 Pa with maintained elastic character (tan δ = 0.35), while Bai et al. [31] documented that konjac glucomannan-curdlan optimal systems reach G' ~3200 Pa with superior tan δ = 0.22 (indicating elastic dominance). The pattern emerges that ionic-crosslinked systems (carrageenan-based) and dual-crosslinked systems (gelatin-carrageenan) achieve the highest G' values, while co-polymer systems with weaker interaction mechanisms (starch-protein isolate) achieve G' ~1500 Pa, limiting their applicability without additional stabilizers.

Loss modulus (G") represents the viscous component enabling flow, but must remain below 1200 Pa in optimal formulations to prevent excessive material spreading. Ahmad et al. [14] employed computational fluid dynamics (CFD) simulations using ANSYS Fluent to model how rheological parameters translate to extrusion pressure and shear rate distributions, validating that modified thixotropic protocols based on actual shear conditions during printing provide accurate predictions of ink performance. The critical insight emerged that KCl-crosslinked kappa-carrageenan inks show excellent multi-layer printability despite lower viscosity recovery (relative to uncrosslinked inks) because elevated mechanical stability imparted by KCl enables effective structural recovery.

3.3. Loss Tangent and Network Elasticity Dominance

The loss tangent (tan δ = G"/G') measures the ratio of dissipated (viscous) to stored (elastic) energy; optimal values below 0.3 signal elastic-dominated networks for shape retention after printing. Agarwal et al. [35] showed that tan δ <0.25 indicates strong elasticity and excellent recovery, 0.25–0.50 is a transition zone with intermediate properties, and >0.50 signals viscous dominance and poor shape retention. De Salvo et al. [36] optimized phytosterol-enriched oleogels, finding that dynamic moduli must support self-structuring: gelation at 78.37°C and storage modulus G' = 3.07±0.032 Pa·s yield good extrusion flow, while G' = 3.07×10^6 Pa ensures room-temperature stability. This shows post-extrusion elastic recovery is a second key printability window.

3.4. Apparent Viscosity and Filament Formation

Apparent viscosity (η) governs filament diameter and geometric resolution (η ∝ filament width). Nguyen et al. [37] determined optimal viscosity for rice protein-starch systems at 1–10 kPa·s, with best printability at 17.5% rice protein and 15% starch. Rapid, reversible recovery in rice protein systems is essential for stable multi-layer deposition without excessive flow or collapse. Dushina et al. [30] quantified viscosity changes: CT-free ink (CT0) increased from 9.6 to 75.4 kPa·s during cooling (50→20°C), while CT80 ink changed only 0.9 to 5.6 kPa·s—a 13-fold reduction in temperature sensitivity. Adding plant callus tissue broadens processing windows but reduces structural integrity by dampening viscoelastic response. Higher volumetric flow rates raise shear stress during extrusion, directly affecting filament geometry and required extrusion pressure.

 doi:10.20944/preprints202603.0723.v1

3.5. Thixotropy, Recovery Kinetics, and Structural Integrity

Thixotropic behavior—shear-thinning under stress and rapid viscosity recovery—enables extrusion at practical pressures and maintains geometric precision after printing. Three-interval thixotropy tests have been widely adopted in food printing studies [5,38]. In these studies, standardized recovery assessments specify that more than 80% deformation and nearly 100% structural recovery indicate optimal printability, whereas less than 50% recovery suggests poor elastic recovery for multi-layer builds. Thixotropy tests evaluate structural integrity by cycling application of low and high deformations, i.e., around 1%, simulating the rest state, whereas 100% and higher, from the printing phase. The key parameter for printability is the gel's recovery kinetics—the rate and extent of structural regeneration after each destructive shear cycle—which ultimately determines its ability to maintain shape fidelity during multi-layer fabrication [5,38,39].

Rodríguez-Herrera et al. [11] identified key recovery parameters for nixtamalized corn doughs: loss tangent at minimum strain and elastic modulus govern recovery kinetics; storage and Young's moduli affect self-support after deposition. Loss tangent at nozzle strain and yield stress control extrusion behavior, while elastic modulus dictates post-printing stability, highlighting that different rheological parameters dominate distinct stages and require multi-stage optimization. Recovery timescales differ widely: optimal formulations regain 80% viscosity within 30 seconds, supporting rapid printing (>300 mm/min); 60-second recovery suits moderate speeds (100–300 mm/min); >100 seconds limits use to slow (<50 mm/min) or single-layer printing.

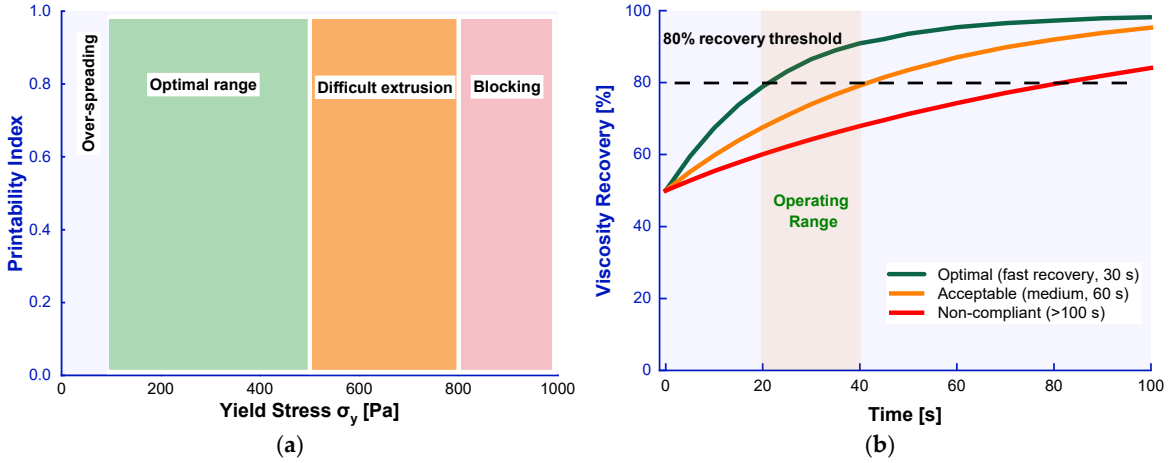

Figure 1. Critical metrics in relation to ink rheological properties affecting 3D food printing: (**a**) Yield stress operating regions; (**b**) Thixotropy recovery post-extrusion.

The following Table summarizes the previously discussed rheological parameters in recent experimental works.

Table 1. Key rheological metrics (G′, G″, η, σy) for experimentally evaluated extrusion-based 3D food-printing formulations. Values are reproduced from the cited studies or digitized/extracted from reported tables and figures.

Ref.	G′ [Pa]	G″ [Pa]	η [Pa·s]	Yield stress [Pa]	System	Note
[7]	446-9707	93-3489	57-1309	181-4392	starch gels + proteins + hydrocolloids	K-index [Pa·s^n]: 57.3 - 912
[11]	200-7x10^4	~50-10^4	~10-10^5	9.4-3220	nixtamalized corn dough	Flour 25%-40%
[26]	1150-6909	100-1400	N/A	32-455	potato starch + plant proteins + carrageenan	-

 doi:10.20944/preprints202603.0723.v1

[28]	~1.00×10^4–1.22×10^4	~1.50×10^3–2.05×10^3	313.48	470.69	mashed potatoes + k-carrageenan + gelatin-B	-
[29]	~1800-1.3x10^4	200-2700	N/A	N/A	fish myofibrillar-protein pastes with oils	for >55 °C, G′ higher for moderate lipids than the oil-free control
[30]	1.34x10^4-2.28x10^4	1750-3380	9600-7.54×10^4	N/A	agar + mashed potato + lupin	-
[33]	~1000–4×10^4	~300–3.0×10^4	~30-8000	N/A	cereal–legume starch-based + hydrocolloid mixture	K-index [Pa·sⁿ]: 500–995
[35]	180-7000	150-800	49-531	18.6-268.7	psyllium husk (PH)/gelatin blends	K-index [Pa·sⁿ]: 49.3 - 530
[36]	~1×10^6–5×10^6	~7.9×10^4–4.0×10^5	~0.013–0.5 & ~1–1000 (*)	NR	phytosterol-enriched monoglyceride (MG) oleogels	(*) as for wt% phytosterols (up to 40%) and shear rates
[37]	~1000–2×10^4	~200–3500	~0.8–5000	N/A	rice protein–corn starch gels (high-amylose)	-
[40]	3.96×10^4-6.09×10^4	~2000-8000	273-2122	268-1803	shiitake mushroom paste with gums (AG/XG/KG)	-
[41]	~6000–4.5×10^4	~2000–8000	1.74×10^3–2.58×10^4	N/A	surimi paste inks with starch–salt–water	starch enhances G′, and G″; water and salt enhance fluidity
[42]	150–3.43×10^4	57.3–8335	160–3.53×10^4	16.6–96.3	rice–black gram idli batter + pearl millet flour	yield stress from Herschel–Bulkley model

4. Process Characteristics and Parameter Optimization

4.1. Nozzle Diameter and Printing Resolution Trade-off

Nozzle diameter is a fundamental geometric parameter in extrusion-based food printing, as it determines the minimum achievable feature size and directly influences deposition accuracy and printing throughput. Smaller nozzles generally enable higher spatial resolution and finer filament deposition but require higher pressure or lower printing speeds to maintain stable flow. Conversely, larger nozzles allow higher deposition rates and reduce the extrusion force needed, although at the expense of printing resolution and geometric fidelity.

In the study by Santhoshkumar et al. [38], three nozzle diameters (0.84, 1.22, and 1.56 mm) were evaluated during the printing of pearl-millet–banana formulations. Printing trials revealed that the 0.84 mm nozzle could not produce printable constructs, due to insufficient flow and clogging, whereas the 1.56 mm nozzle resulted in over-extrusion and thick filament deposition. In contrast, the 1.22 mm nozzle provided the best compromise between extrusion stability and printing accuracy. When printing speeds of 600–1000 mm/min were evaluated, stable extrusion through the 1.22 mm nozzle at 600 mm/min generated deposition rates of approximately 0.33–0.37 g/min, whereas higher speeds caused under-extrusion and discontinuous filaments.

The optimal printing window therefore depended on the interaction between nozzle diameter and material rheology. The millet–banana formulations exhibited shear-thinning behavior ($n \approx 0.02$–0.40) with viscosity ranging from 10^5 Pa.s to a few Pa.s (for infinitesimal shear rate to 100 s^{-1}), yield stresses of 10–80 Pa and storage moduli of 2000–6000 Pa, properties that supported extrusion while maintaining filament stability after deposition. Beyond nozzle diameter, the nozzle–substrate gap (commonly referred to as layer height) also affects the final filament geometry. The final printed line width and height are not determined solely by nozzle diameter but by the interaction between nozzle geometry, extrusion rate, travel speed, and the rheological recovery behavior of the food ink. When extrusion rate, printing speed, and nozzle geometry are not properly balanced, deformation regimes

 doi:10.20944/preprints202603.0723.v1

of stretching and compression appear [38]. Consequently, the rheological characteristics govern the three main stages of extrusion-based food printing—extrusion, structural recovery, and self-supporting stabilization—which collectively determine the printability of food formulations [23].

Another critical phenomenon associated with nozzle geometry is die swell, which occurs when viscoelastic materials expand after exiting the nozzle due to elastic recovery of polymeric or protein networks that were stretched during flow. In extrusion-based food printing, die swell alters the final filament diameter and therefore affects the relationship between the nozzle diameter and the printed line width. Finite-element modeling of surimi paste, supported by rheological data, demonstrated that die swell increased from approximately 9.8% to 14.1% as nozzle diameter decreased from 1.2 to 0.6 mm, due to higher pressure gradients and stored elastic energy within the material during extrusion [43].

Overall, nozzle diameter must be optimized together with printing speed, extrusion rate, layer height, and material rheology to balance resolution, extrusion stability, and structural retention. Smaller nozzles enhance printing precision but increase pressure requirements and susceptibility to flow instabilities, whereas larger nozzles improve throughput and extrusion reliability but limit geometric resolution.

4.2. Printing Speed, Layer Height, and Dimensional Accuracy

Printing speed controls deposition rate and inter-layer bonding, with optimal values highly formulation-dependent. Santhoshkumar et al. [38] found pearl millet-banana inks performed best at 600 mm/min, 360 rpm motor speed, and 1.22 mm nozzle, achieving 92% accuracy. In contrast, butterfly pea flower inks required 40 mm/min for optimal results, indicating that less elastic, slower inks need reduced speeds for precision. Reducing layer height from 1.0 mm to 0.2 mm increases accuracy from 75–82% to 97–99%. The optimal range (0.3–0.5 mm) yields 96–98% accuracy with efficient processing. Heights below 0.2 mm show diminishing returns, demanding more pressure and time without proportional gains. Optimal print quality is achieved when the nozzle diameter-to-layer height ratio is 0.5–0.55, offering an empirical guideline for parameter selection. Post-printing shape changes reveal that infill levels strongly affect dimensions and hardness: 40% infill produces 37% lower hardness than 100% due to greater porosity. Fermentation-driven shape change also correlates with infill pattern, underscoring the need for integrated optimization of design and post-processing. Table 2 presents the extrusion-based 3D food-printing process parameters reported in experimental studies.

Table 2. Printing settings reported in experimental extrusion-based 3D food-printing studies (print-quality metric as defined in each study).

Ref.	Nozzle Diameter (mm)	Printing Speed (mm/min)	Layer Height (mm)	Extrusion Rate (mm^3/s)	Printing Accuracy (%)
[7]	1.0	1200 (20 mm/s)	1.0	2.2%	N/A
[11]	2.0	1200 (20 mm/s)	2.0	N/A	N/A
[28]	1.2	1500 (25 mm/s)	1.2	N/A	N/A
[33]	1.2	1500 (25 mm/s)	0.84	N/A	SSI (%) > 99
[36]	0.83	60–360 (1–6 mm/s)	1.0	N/A	N/A
[37]	0.8, 1.5, 2.5	3200 (53 mm/s)	1.4	5.7, 6.3, 6.9 mL/min	cylinder volume
[40]	1.2	1500 (25 mm/s)	1.2	N/A	N/A
[41]	1.94	900 (15 mm/s)	1.2	5.75 (actual)	layer sharpness ~39.8% to 55.8%
[42]	1.22	400–1400	various	7.8 to 27.3	shape evaluation
[43]	1.0	900 (15 mm/s)	1.0	25	N/A
[44]	1, 1.5, 2, 2.5, 3	1800 – 4200 (30–70 mm/s)	N/A	N/A	N/A

 doi:10.20944/preprints202603.0723.v1

4.3. Temperature Control and Thermal Stability

Processing temperature modulates viscosity, gelation kinetics, and bioactive stability, requiring careful balance specific to each ink formulation. Distinct optimal temperatures exist for different material classes: starch-based inks optimize at ~25°C (room temperature, minimizing viscosity change while avoiding starch granule swelling), while protein-based inks optimize at ~60°C (enhancing protein functionality while maintaining adequate flow properties). Nguyen et al. [37] achieved optimal rice protein-starch system performance at 60°C, demonstrating rapid and reversible response characteristics enabling multi-layer printing. The critical safe temperature range spans 40-60°C, avoiding thermal degradation of sensitive compounds (anthocyanins, polyphenols, probiotics) while maintaining adequate rheological properties for extrusion. Above 70°C, accelerated degradation of sensitive compounds occurs.

4.4. Extrusion Parameters and Filament Uniformity

Extrusion rate (volumetric flow) controls filament diameter and structural consistency. Optimal extrusion parameters differ by food ink type, with extrusion rate reflecting material properties. Motor speed (rpm) sets the pump's rotation and volumetric output. Studies show that optimal motor speed must be paired with nozzle size and print speed; actual delivery rate depends on motor speed and pump geometry, requiring experimental calibration for each printer setup. Santhoshkumar et al. [38] found that pearl millet-fortified formulations achieve optimal printability and stability at specific extrusion rates, printing speeds, and nozzle sizes. The linear relationship between extrusion rate and filament diameter allows precise prediction of filament size from the set extrusion rate [44].

4.5. Multi-Parameter Optimization and Interaction Effects

Nozzle diameter, printing speed, layer height, and extrusion rate interact, requiring simultaneous—not sequential—optimization. Optimal results occur at 300–400 mm/min printing speeds and 6–10 mm^3/s extrusion rates, balancing processing speed and structural quality. Central composite design systematically optimizes extrusion parameters by evaluating multiple factors. Principal component analysis groups samples, revealing high print fidelity at specific nozzle diameters, extrusion rates, speeds, and layer heights. Response surface methodology and statistical design of experiments offer robust frameworks for uncovering parameter interactions [37,41,44]. Machine learning optimization, using grey relational analysis of multiple objectives, identifies and validates optimal parameter combinations with low experimental error rates versus theoretical predictions. Data-driven frameworks thus offer practical, efficient tools for parameter optimization without exhaustive experimental trials.

4.6. Printing Accuracy and Fidelity Metrics

Printing accuracy measures how closely fabricated structures match digital designs, assessed by dimensional and image analysis. Among food inks, cereal-legume starch gels yield the highest accuracy (99.37%), specialty systems reach 98% and 96%, while chocolate-based inks lag at 88% due to thermal sensitivity and viscosity-temperature complexities. These differences highlight the challenge of ensuring structural stability across material types. Systematic quality assessment of 3D-printed cereal products identifies key parameters: ink mechanical properties, printed object shapes (e.g., image analysis, calculations), and final products via microscopy, instrumental, and sensory texture evaluation [45,46]. This framework shows that printability covers not only initial dimensional accuracy but also long-term stability and sensory quality after processing. In the context of 3D food printing, resolution determines the structural fidelity and surface smoothness of edible constructs, directly influencing both the sensory "mouthfeel" and the precision of intricate internal geometries [47,48]. By optimizing nozzle diameters and layer heights, we can minimize visible layering to achieve the refined textures and tight tolerances essential for complex, multi-component food designs

 doi:10.20944/preprints202603.0723.v1

[44–46]. The interrelation between critical ranges of process parameters and rheological parameters is shown in Figure 2.

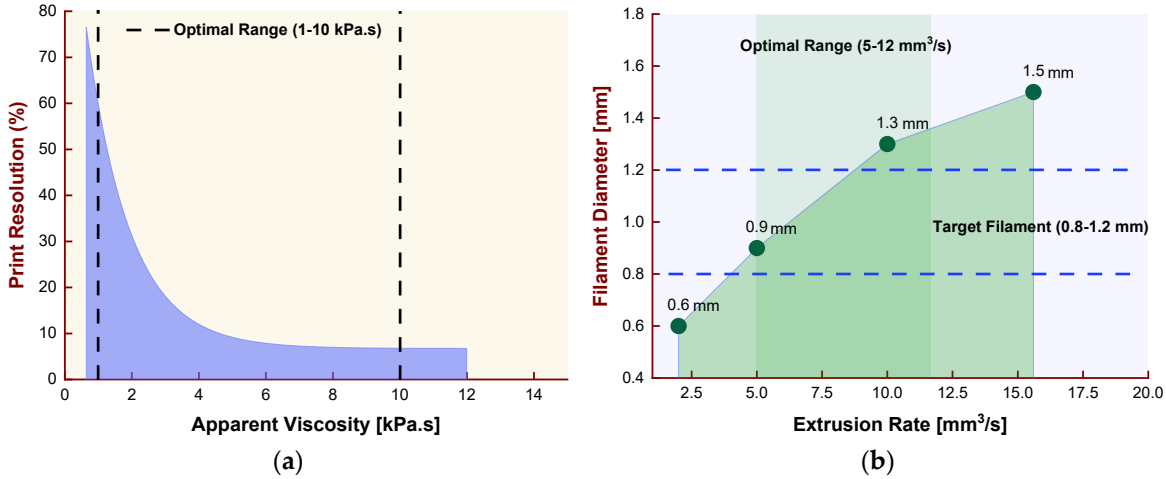

Figure 2. Process parameters and rheological properties governing 3D food fine printability: (**a**) Interrelation of ink viscosity and resolution; (**b**) Filament diameter and extrusion rate.

Accurate dimensional prediction depends on integrating material rheology and process parameters. Combining experimental tests, numerical modeling, and neural networks allows optimization by classifying filament deposition into regimes: quasi-Newtonian flow, round deposition, spreading, tearing, and layer-pressing. This approach explains how rheology (yield stress, plastic viscosity) and process variables (nozzle diameter, height, speed, extrusion velocity) shape filament geometry—directly informing food printing optimization.

5. 4D: Post-Printing Treatment and Temporal Activation of Printed Structures

Four-dimensional (4D) food printing extends extrusion-based 3D printing by integrating triggered changes into the printed construct, where functionality evolves after fabrication through controlled activation (e.g., time-dependent transformations). In food systems, the "fourth dimension" is most often expressed not as dramatic shape morphing alone, but as post-printing consolidation and stimulus-triggered changes in mass transfer, including delayed hydration, programmed softening, controlled color transitions, and staged bioactive release. This behavior emerges from coupled design of material formulation, printed architecture (e.g., infill and porosity), and post-printing treatments, which together define activation kinetics and the stability of nutrients and bioactives [49–51].

5.1. Thermal Post-Processing as Activation: Structure Consolidation and Bioactive Preservation

Thermal post-processing functions as an activation step that can consolidate printed networks through starch gelatinization and protein crosslinking, while simultaneously altering moisture content and diffusion pathways. In butterfly pea flower (BPF)-based printed structures, steaming maintained higher dimensional fidelity than water-immersion cooking or oven heating and supported strong bioactive preservation. Quantitatively, steaming achieved 91–97% anthocyanin retention, whereas microwave drying produced 74–85% retention, demonstrating that processing route selection can shift bioactive losses by more than ten percentage points within a single formulation class [52].

Moisture loss is a critical activation variable because it governs both mechanical evolution and transport control. Documented thermal treatment led to 35.6% weight reduction (water loss) in food systems, correlating with network consolidation and controlled moisture gradients that enable timed release behavior [42]. In aronia-loaded printed gels, thermal treatment is reported to trigger starch gelatinization and protein network formation, which subsequently governs the release rate of

 doi:10.20944/preprints202603.0723.v1

polyphenols (including anthocyanins) during gastrointestinal digestion [53]. In this activation logic, thermal treatment reduces early-stage diffusion (by tightening the gel network and reducing free water) while supporting later-stage release when environmental conditions (e.g., intestinal pH) become favorable for solubilization and absorption [53].

Activation timescales vary with the target outcome and geometry. Reported thermal treatment durations range from minutes (rapid steaming; ~5–10 min for small constructs) to tens of minutes or longer (slow oven drying; ~45–90 min for broader moisture control), reflecting the need to match treatment duration to construct size, internal design, and desired post-printing evolution pathway [51,52].

5.2. Fermentation-Driven Activation: Time-Programmed Softening, Porosity Effects, and Nutritional Evolution

Fermentation provides a biological activation route that can reshape texture and internal structure without external physical triggers, while simultaneously altering nutritional and sensory attributes. In printed idli batter systems, time-dependent changes were linked explicitly to architecture and formulation. Hardness reduction and shape change scaled with infill: constructs printed at 40% infill showed 37% lower hardness than 100% infill, consistent with increased porosity and lower structural density [42]. Formulation also modulates fermentation kinetics. Pearl millet fortification at 20% (w/w) accelerated fermentation, increasing acid production and amplifying fermentation-driven changes relative to controls [42]. A practical process window was reported: most food inks require 12–36 h at 30–40°C, while fermentation beyond 48 h increases the risk of degradation or contamination, and fermentation shorter than 12 h may yield incomplete changes in structure and nutritional endpoints [42]. Fermentation-oriented 4D mechanisms are therefore architecture-dependent: printed geometry determines gas retention and pore evolution, while formulation governs microbial activity and matrix susceptibility. This also motivates integration with broader fermentation innovation in plant-based foods, where microbial metabolism can be used alongside printing to steer sensory profile development and functional performance over time [54].

5.3. Digestive-Environment Activation: pH, Ionic Strength, Hydration, and Staged Release

A significant portion of food-relevant 4D behavior aligns naturally with gastrointestinal stimuli, where hydration and chemical gradients serve as intrinsic activators. pH-responsive mechanisms regulate swelling, deswelling, relaxation, and electrostatic interactions, enabling staged release during transitions from the stomach to the intestine. The efficacy of such digestive-environment activation is intrinsically linked to the printed product's internal architecture. As reviewed by Lombardi et al. [55], the controlled design of hierarchical porosity—combining macro- and micro-scale pores—can modulate enzyme penetration and diffusion pathways, thereby directly influencing the kinetics of nutrient release and matrix degradation. This positions porosity not just as a textural element, but as a tunable parameter for governing bio-accessibility in 4D-printed foods. Beyond simple shape transformation, 4D printing with zein-based specimens utilizes the water-driven self-assembly of hydrophobic fibrils to achieve temporal functional heterogeneity in both degradation and release kinetics [56]. Notably, Zhang et al. [56] demonstrated that by modulating the composition of the supporting bath, this behavior can be finely tuned: conduits printed in 75% water exhibit a porous architecture that results in 88.2 ± 1.17% degradation over 10 days under protease XIV exposure, while 40% water baths yield more compact structures that limit enzyme penetration and provide significantly lower degradation with stable wall thickness.

Ionic responsiveness provides a parallel activation mechanism because salts and pH gradients in digestive fluids modify polymer hydration, crosslinking balance, and network stability. In a food-printing context, coaxially printed starch/alginate–pectin hydrogels showed pH-responsive behavior and maintained structural fidelity while enabling encapsulation functionality, demonstrating how edible printed hydrogels can be designed for environment-dependent integrity and release [57]. Pectin hydrogels provide a clear pH-linked quantitative framework for food-relevant behavior:

 doi:10.20944/preprints202603.0723.v1

gelation is inhibited under acidic gastric conditions (around pH 2.0–3.0), becomes favorable in the small intestine (pH 6.0–6.5), and can further consolidate in the colon-like range (pH 7.5–8.0), enabling environment-dependent control over integrity and release [58].

Emulsion gels extend this logic by coupling interfacial stability with digestive conditions. Protein–polysaccharide complexes that stabilize emulsion gel inks are modulated by pH-dependent electrostatic interactions, enabling programmed gel formation or breakdown and supporting controlled release of hydrophobic bioactives through digestion-linked interfacial changes [59]. Within a 4D framework, these systems support sequential responses: constructs can remain stable through early exposure and activate later through hydration, pH shifts, ionic changes, and enzymatic action, yielding time-dependent release profiles rather than a single-step response [49].

5.4. Multi-Stimulus Systems and Application Targets: From Delivery to Medical Nutrition

Multi-stimulus designs combine physical consolidation (thermal), biological remodeling (fermentation), and digestive triggers (pH/ionic strength/hydration) to achieve programmable performance. Bigel architectures—hydrogel–oleogel hybrids—provide an additional design degree of freedom by separating hydrophilic and lipophilic domains, enabling dual-phase control where the hydrogel governs water-driven transport and the oleogel supports lipophilic protection and enzymatic breakdown pathways [60].

Application-driven 4D food printing emphasizes functional outcomes that evolve over time: improved stability of sensitive compounds during processing and storage, followed by controlled bioaccessibility during digestion [53]. The evaluation of final product functionality—nutritional and sensory—is vital for the impact of 3D-printed foods. Herdeiro et al. [61] assessed snacks with edible insect meals (*Tenebrio molitor, Alphitobius diaperinus*), providing key post-printing data: protein content reached ~14 g/100g, antioxidant capacity increased (DPPH from 3.53 to 9 μmol TEAC/g for *A. diaperinus*), and sensory scores were acceptable (~4.5–4.9/9). These quantitative results in nutrition and palatability illustrate the 'evolved state' 4D printing seeks, stressing the importance of future strategies that deliver both physiological benefits and consumer acceptance. Similarly, an effort to develop a snack cracker that utilizes imperfect vegetables (3D-printed snacks from upcycled broccoli and carrot powders) as alternative ingredients that add value both nutritionally and economically has also been reported [62].

Medical nutrition provides a strong target domain, including texture-managed foods designed for safe swallowing and improved palatability, where printed architecture and post-processing jointly govern time-dependent softening and stability Wang et al. [63]. The internal structural design of printed products—including infill density, layer orientation, and compartmentalization—critically determines quality retention and nutritional preservation during post-processing interventions [63], as demonstrated in dysphagia applications [40,64–67]. Sesame oil bodies (SOBs) have recently attracted attention in dysphagia-oriented food design because they naturally contain bioactive compounds and exhibit suitable rheological behavior for extrusion-based printing [68,69]. Such lipid–protein structures enable the formulation of soft-textured foods with improved nutritional value while maintaining printability. Protein-based inks and plant-based meat analog formulations further extend this concept by enabling formulation-driven control of network architecture and post-processing texture development.

5.5. Emerging Multiphase Architectures for Functional 3D Food Printing

The research efforts and the systems discussed in this section are considered as advanced interfacial/multiphase strategies for tuning printability and post-printing functionality.

Coaxial food printing

Multiphase structuring approaches such as coaxial extrusion have expanded the functional capabilities of food printing. Emulsion gels and bigels—biphasic systems combining hydrogel and oleogel phases—have emerged as promising printable materials and fat mimetics [70–75]. These

 doi:10.20944/preprints202603.0723.v1

systems provide simultaneous control of hydrophilic and lipophilic domains, improving mechanical strength and structural stability. For example, Johansson et al. [76] demonstrated that pea-protein-based bigels can be used for single-, dual-, and coaxial-material printing, producing structures with enhanced mechanical integrity. Comparable improvements in structural stability have also been reported for other emulsion-gel formulations [77].

Gels utilizing nanoparticles and nanorods

Nanostructured stabilizers further enhance food inks. Starch nanoparticles can be used to stabilize emulsions because they can adsorb at the oil–water interface, forming physical barriers, hence causing a reduction in droplet interactions [78]. They can also interact with carrageenan, a colloidal polysaccharide, forming 3D gel networks, thereby empowering system stability and mechanical strength [79]. Starch nanorods (SNRs) have been synthesized at different aspect-ratio shapes with the aid of alkaline hydrolysis-nanoprecipitation facilitated by thermal regulation, as reported by Chen et al. [80] and Ruan et al. [81]. Starch nanorods (SNRs) with prismatic, ellipsoidal, and spindle-shaped morphologies have also been employed to stabilize docosahexaenoic acid (DHA)-rich algal oil emulsion gels as reported by Zhong et al. [82].

Protein-based Pickering emulsion 3D printing

Pickering-emulsion-based 3D printing represents another emerging strategy. This method uses stable Pickering emulsions as inks for the creation of complex food structures with high precision [83,84]. Layer-by-layer deposition is being used for control of shape and function [85–87]. Pickering emulsion stability and rheology can be improved with the aid of Xanthan gum (XG), a natural polysaccharide. If combined with proteins, XG forms stable interfacial networks, increasing phase viscosity [88,89]. Marine protein-based platforms such as mussel adhesive protein (MAP), a natural biopolymer rich in 3,4-dihydroxyphenylalanine (DOPA) combined with xanthan gum (XG) were employed to stabilize Pickering emulsion gels and showed long-term stability and reliable printability [90].

6. Outlook: Multi-Parameter Interactions in 3D/4D Food Printing

Successful 3D food printing depends on optimizing three interconnected domains: (1) Network Architecture, which sets fundamental gel properties via formulation; (2) Critical Rheological Properties, which control material flow and recovery; and (3) Process Characteristics, which translate material properties into fabrication outcomes.

Critical parameters—such as storage modulus, yield stress, viscosity, loss tangent, nozzle diameter, printing speed, layer height, extrusion rate, starch, and water content—jointly determine printing outcomes. Secondary factors (loss modulus, print temperature, extrusion pressure, protein, and hydrocolloid content) further refine these effects. Optimal parameter ranges are material-specific, necessitating experimental validation for new formulations.

Multi-parameter interactions are critical: G' enhances stability, while yield stress avoids spreading and extrusion issues. Smaller nozzles require slower speeds and lower viscosities; higher printing speeds (>400 mm/min) with low-viscosity inks risk filament thinning unless a high G' is maintained. Small layer heights demand higher G' for structure, and starch content below 20% undermines network strength, whereas the upper limit should be particularly identified. Complex, multi-component systems, such as ionic-crosslinked and dual-crosslinked systems, deliver superior mechanical properties at the cost of increased complexity. Processing parameters—such as printing speeds and nozzle diameters—vary up to 50-fold across formulations, making formulation-specific optimization essential.

In the framework presented here, multi-parameter optimization—formulation, rheology, and process conditions—enables precise 3D printing and forms the basis for 4D food printing, where post-printing stimuli activate time-dependent structural and functional changes. This progression connects static fabrication to dynamic, programmable food constructs.

This framework shows that 3D/4D food printing success depends on:

 doi:10.20944/preprints202603.0723.v1

- Higher G' generally increases stability and stacking accuracy (G' >4000 Pa), but excessive stiffness impairs extrudability unless balanced by strong shear thinning.
- Low Yield Stress causes spreading; above 500 Pa, extrusion is difficult. Most formulations perform best at 100–300 Pa.
- Nozzle diameter and printing speed are interdependent: smaller nozzles require slower speeds and lower viscosities; larger nozzles handle higher viscosities and faster deposition rates.
- Printing speeds above 400 mm/min with low-viscosity inks risk filament thinning and collapse unless elasticity is maintained (G' >2000 Pa).
- Layer heights below 0.3 mm can improve fidelity but require strong elastic recovery, typically from higher G'.
- Starch content above 30% restricts extrudability; below 20% weakens the network and reduces stability.

Integrating formulation, rheology, and processing builds a comprehensive framework that advances 3D/4D food printing toward commercial and multi-material applications.

Critical Research Gaps and Future Directions

Current literature employs diverse rheological measurement protocols, making direct comparison across research efforts challenging. The field would benefit substantially from the development of standardized measurement protocols, critical threshold values for key parameters, multi-parameter printability indices, and process-relevant measurement conditions. While individual publications demonstrate specific formulation-property linkages, comprehensive maps of how formulation variables systematically affect network architecture and printing performance remain unfinished. Future research should develop high-throughput formulation screening, quantitative composition-property maps, material selection frameworks, and cross-material comparison studies. Although current research efforts tend to address network characterization and process optimization together, a great section of effort still tackles these separately. Integration would require coupled formulation-process optimization, machine learning models, dynamic measurement approaches, and real-time feedback control systems. While biomedical 4D printing applications have advanced substantially, food-specific applications remain underdeveloped. Priority research areas include personalized nutrition, dysphagia-adapted foods, food waste reduction, regulatory pathways for 3D-printed food products, and scalability and economics demonstrations.

Author Contributions: Conceptualization, T.G. and T.V.; methodology, T.G. and T.V.; validation, T.G. and T.V.; resources, T.G. and T.V.; writing—original draft preparation, T.G. and T.V.; writing—review and editing, T.G. and T.V.; visualization, T.G. and T.V. All authors have read and agreed to the published version of the manuscript.

Funding: This research received no external funding.

Data Availability Statement: Supporting data are available upon request.

Conflicts of Interest: The authors declare no conflicts of interest.

References

1. Qin, Z.; Yang, Y.; Zhang, Z.; Li, F.; Hou, Z.; Li, Z.; Shi, J.; Shen, T. A critical review: gel-based edible inks for 3D food printing—materials, rheology-geometry mapping, and control. *Gels* **2025**, *11(10)*, 780. https://doi.org/10.3390/gels11100780
2. Herrada-Manchón, H.; Fernandez, M.A.; Aguilar, E. Essential guide to hydrogel rheology in extrusion 3D printing: how to measure it and why it matters. *Gels* **2023**, *9(7)*, 517. https://doi.org/10.3390/gels9070517
3. Fragal, E.H.; Poirier, A.; Bleses, D.; Silva, Y.F.G.; Baccile, N.; Rharbi, Y. Microbial biosurfactant hydrogels with tunable rheology for precision 3D printing of soft scaffolds. *Soft Matter* **2025**, *21(22)*, 4476-4487. https://doi.org/10.1039/D5SM00248F

 doi:10.20944/preprints202603.0723.v1

4. Fahmy, A.R.; Derossi, A.; Jekle, M. Four-Dimensional (4D) printing of dynamic foods—Definitions, considerations, and current scientific status. *Foods* **2023**, *12*, 3410. https://doi.org/10.3390/foods12183410
5. Heckl, M.P.; Korber M.: Jekle, M.; Becker T. Relation between deformation and relaxation of hydrocolloids-starch based bio-inks and 3D printing accuracy. *Food Hydrocoll.* **2023**, *137*, 108326. https://doi.org/10.1016/j.foodhyd.2022.108326
6. Liu, W.; Chen, L.; McClements, D.J.; Peng, X.; Jin, Z. Recent trends of 3D printing based on starch-hydrocolloid in food, biomedicine and environment. *Crit. Rev. Food Sci. Nutr*. **2024**, *64(26)*, 8948-8962. https://doi.org/10.1080/10408398.2023.2205524
7. Nikolaou, E.N.; Apostolidis, E.; Nikolidaki, E.; Karvela, E.; Stergiou, A.; Kourtis, T.; Karathanos, V.T. The development and optimization of extrusion-based 3D food printing inks using composite starch gels enriched with various proteins and hydrocolloids. *Gels* **2025a**, *11(8)*, 574. https://doi.org/10.3390/gels11080574
8. Taqdissillah, D.; Irsyad, M.; Whulanza, Y. Development of sago starch-alginate hydrogels for extrusion-based 3D food printing. *East.-Eur. J. Enterp. Technol*. **2025**, *4(11)*, 31–41. https://doi.org/10.15587/1729-4061.2025.336896
9. Chen, Y.; Zhang, M.; Bhandari, B. 3D printing of steak-like foods based on textured soybean protein. *Foods* **2021**, *10(9)*, 2011. https://doi.org/10.3390/foods10092011
10. Afnan, Z.; Khalid, U.; Ali, Z.; Khalid, F. Plant based ingredients in 3D food printing: A sustainable approach to personalized nutrition. *Haya Saudi J. Life Sci.* **2025**, *10*, 606-617. https://doi.org/10.36348/sjls.2025.v10i10.007
11. Rodríguez-Herrera, V.V.; Umeda, T.; Kozu, H.; Sasaki, T.; Kobayashi, I. Printability of nixtamalized corn dough during screw-based three-dimensional food printing. *Foods* **2024**, *13(2)*, 293. https://doi.org/10.3390/foods13020293
12. Xu, M.; Dong, Q.; Huang, G.; Zhang, Y.; Lu, X.; Zhang, J.; Zhang, K.; Huang, Q. Physical and 3D printing properties of arrowroot starch gels. *Foods* **2022**, *11(18)*, 2854. https://doi.org/10.3390/foods11142140
13. Mishra, A.A.; Chandregowda, M.; Fai, J.; et al. Tunable elasto-viscoplastic properties of polymer blends for 3D printing applications. *Macromol. Rapid Commun.* **2025**, *46(11)*, 2500249. https://doi.org/10.1002/marc.202500249
14. Ahmad, S.; Alam, H.; Thareja, P. 3D Printing of hydrogels: A synergistic approach of rheology and computational fluid dynamics (CFD) modeling. *RSC Adv.* **2025**, *15*, 39369-39390. https://doi.org/10.1039/d5ra04380h
15. de Farias, P.M.; Matheus, J.R.V.; Maniglia, B.C. et al. Bibliometric mapping analysis of Pickering emulsion applied in 3D food printing. *Int. J. Food Sci. Technol.* **2024**, *59(4)*, 2186–2196. https://doi.org/10.1111/ijfs.17040
16. Ahmadzadeh, S.; Barekat, S.; Ubeyitogullari, A. Enhancing lutein and anthocyanins stability and bioaccessibility through simultaneous encapsulation using coaxial 3D food printing. *NPJ Sci. Food* **2025**, *9(1)*, 96. https://doi.org/10.1038/s41538-025-00439-2
17. Dou, X.; Ren, J. The application of dairy products and their derivatives as edible inks in 3D printing technology: A review. *Int. J. Food Sci*. **2024**, *59(11)*, 8630-8644. https://doi.org/10.1111/ijfs.17195
18. Azman, N.Y.; Fuzi, S.; Abdul Manas, N.H. Development of cellulose based food-ink from cellulose powder. *Food Research* **2024**, *8(2)*, 16-21. https://doi.org/10.26656/fr.2017.8(2).104
19. Yu, J. Personalized delivery of probiotics and prebiotics via 3D food printing. *Metabolites* **2025**, *15(10)*, 642. https://doi.org/10.3390/metabo15110744
20. Domalska, Z.; Jakubczyk, E. Characteristics of food printing inks and their impact on selected product properties. *Foods* **2025**, *14*, 393. https://doi.org/10.3390/foods14030393
21. Agunbiade, A.O.; Song, L.; Agunbiade, O.J.; et al. Potentials of 3D extrusion-based printing in resolving food processing challenges: A perspective review. *J. Food Process Eng.* **2022**, *45(4)*, e13996. https://doi.org/10.1111/jfpe.13996
22. Kadival, A.; Kour, M.; Meena, D. et al. Extrusion-based 3D food printing: Printability assessment and improvement techniques. *Food Bioprocess Technol.* **2023**, *16*, 987–1008. https://doi.org/10.1007/s11947-022-02931-z

 doi:10.20944/preprints202603.0723.v1

23. Derossi, A.; Spence, C.; Corradini, M.G. et al. Personalized, digitally designed 3D printed food towards the reshaping of food manufacturing and consumption. *NPJ Sci Food* **2024**, *8*, 54. https://doi.org/10.1038/s41538-024-00296-5
24. Seol, J.; Kim, J.; Hong, Y.; et al. Toward intelligent 3D food printing: a review on the perspective of materials, fabrication, monitoring, and control. *Crit. Rev. Food Sci. Nutr.* **2025**, *65(3)*, 546–562. https://doi.org/10.1080/10408398.2025.2538546
25. Chen, Y.; Bi, S.; Gu, J.; Che, Q.; Liu, R.; Li, W.; Dai, T.; Wang, D.; Zhang, X.; Zhang, Y. Achieving personalized nutrition for patients with diabetic complications via 3D food printing. *Int. J. Bioprinting* **2024**, *10(2)*, 1862. https://doi.org/10.36922/ijb.1862
26. Nikolaou, E.N.; Karvela, E.; Apostolidis, E.; Karathanos, V.T. Effects of different mechanical processing methods on physicochemical properties of potato starch-plant protein-carrageenan composite gels. *Food Measure*. **2025b**, *19*, 2926–2941. https://doi.org/10.1007/s11694-025-03156-2
27. Kaliampakou, C.; Lagopati, N.; Charitidis, C.A. Direct ink writing of alginate-gelatin hydrogel: An optimization of ink property design and printing process efficacy. *Appl. Sci.* **2023**, *13(14)*, 8261. https://doi.org/10.3390/app13148261
28. Li, Y.; Cheng, Z.; Zhang, J.; Xu, S.; Cai, Y.; Ding, Y.; Lyu, F. Effect of protein-polysaccharide hybrid gelator system on the material properties and 3D extrusion printability of mashed potatoes. *J. Food Sci.* **2024**, *89(4)*, 2347–2358. https://doi.org/10.1111/1750-3841.17003
29. Oyinloye, T.M.; Yoon, W.B. Impact of saturated and unsaturated oils on the nonlinear viscoelasticity, microstructure, and 3D printability of fish myofibrillar-protein-based pastes and gels. *Gels* **2025**, *11(4)*, 295. https://doi.org/10.3390/gels11040295
30. Dushina, E.; Popov, S.; Zlobin, A.I.; Martinson, E.; Paderin, N.; Vityazev, F.; Belova, K.; Litvinets, S. Effect of homogenized callus tissue on the rheological and mechanical properties of 3D-printed food. *Gels* **2024**, *10(1)*, 42. https://doi.org/10.3390/gels10010042
31. Bai, C.; Liu, R.; Shen, L.; Yu, Z.; Hu, J. Effects of konjac glucomannan and curdlan on the 3D printability and physicochemical properties of germinated brown rice gel. *Foods* **2025**, *14*, 1764. https://doi.org/10.3390/foods14101764
32. Oliveira, S.M.; Fasolin, L.H.; Vicente, A.A.; Fuciños, P.; Pastrana, L.M. Printability, microstructure, and flow dynamics of phase-separated edible 3D inks. *Food Hydrocoll.* **2020**, *109*, 106120. https://doi.org/10.1016/j.foodhyd.2020.106120
33. Liu, R.; Yu, Z.; Song, J.; Shen, L.; Yin, Y. Evaluation of 3D printing of cereal-legume starch-based gels formulated with red adzuki bean and germinated brown rice flour. *Foods* **2025**, *14(10)*, 1791. https://doi.org/10.3390/foods14101791
34. Choudhury, D.B.; Kumari, S.; Hazarika, M.K. 3D printed sweets made with peanut chenna and milk: A new frontier in food technology. *J. Food Process. Eng*. **2024**, *47(1)*, e14528. https://doi.org/10.1111/jfpe.14528
35. Agarwal, P.; Poddar, S.; Varshney, N.; et al. Printability assessment of psyllium husk (isabgol)-gelatin blends using rheological and mechanical properties. *J. Biomater. Appl.* **2021**, *35(9)*, 1132-1142. https://doi.org/10.1177/0885328220979473
36. De Salvo, M.I.D.; Palla, C.A.; Cotabarren, I.M. Development of an operational map for the 3D printing of phytosterol-enriched oleogels: rheological insights and applications in nutraceutical design. *Gels* **2025**, *14(2)*, 200. https://doi.org/10.3390/foods14020200
37. Nguyen, T.; Ahmadzadeh, S.; Schöberl, H.; Ubeyitogullari, A. Optimizing printability of rice protein-based formulations using extrusion-based 3D food printing. *Food Sci. Nutr*. **2024**, *13(1)*, e4713. https://doi.org/10.1002/fsn3.4713
38. Santhoshkumar, P.; Raja, V.; Priyadarshini, S.R.; Moses, J.A. Evaluating the 3D printability of pearl millet flour with banana pulp blends. *J. Sci. Food Agric.* **2024**, *104(12)*, 7010–7023. https://doi.org/10.1002/jsfa.13389
39. Bercea, M. Rheology as a tool for fine-tuning the properties of printable bioinspired gels. *Molecules* **2023**, *28(6)*, 2766. https://doi.org/10.3390/molecules28062766
40. Liu, Z.; Bhandari, B.; Guo, C.; Zheng, W.; Cao, S.; Lu, H.; Mo, H.; Li, H. 3D printing of shiitake mushroom incorporated with gums as dysphagia diet. *Foods* **2021**, *10(9)*, 2189. https://doi.org/10.3390/foods10092189

 doi:10.20944/preprints202603.0723.v1

41. Lee, J.B.; Yoon, N.Y.; Bae, Y.J.; et al. Optimizing 3D food printing of surimi via regression analysis: Physical properties and additve formulations. *Foods* **2025**, *14(5)*, 889. https://doi.org/10.3390/foods14050889
42. Raja, V.; Moses, J.A.; Anandharamakrishnan, C. Effect of 3D printing conditions and post-printing fermentation on pearl millet fortified *idli*. *J. Sci. Food Agric.* **2022**, *103(4)*, 2145–2154. https://doi.org/10.1002/jsfa.12410
43. Oyinloye, T.M.; Yoon, W.B. Investigation of flow field, die swelling, and residual stress in 3D printing of surimi paste using the finite element method. *Innov. Food Sci. Emerg. Technol.* **2022**, *78*, 103008. https://doi.org/10.1016/j.ifset.2022.103008
44. Soni, R.; Bhandarkar, V.V.; Ponappa, K.; Tandon P. 3D extrusion printability of corn starch and optimization of process parameters for optimal food layered manufacturing. *Manuf. Lett.* **2025**, *44*, 948–957. http://doi.org/10.1016/j.mfglet.2025.06.112
45. Čukelj Mustač, N.; Pastor, K.; Kojić, J. et al. Quality assessment of 3D-printed cereal-based products. *LWT* **2023**, *184*, 115065. https://doi.org/10.1016/j.lwt.2023.115065
46. Uribe-Alvarez, R.; Crofton, E.; Kilcawley, K.; Skibinska, I.; Coleman-Vaughan, C.; Murphy, C.P.; O'Shea, N. Sensory characterisation and volatile analysis of 3D-printed dairy protein-based snack structures. *Int. J. Food Prop.* **2025**, *28(1)*. https://doi.org/10.1080/10942912.2025.2573182
47. Liu, Z.; Zhang, M.; Bhandari, B.; Wang, Y. 3D printing: Printing precision and application in food sector. *Trends Food Sci. Technol.* **2017**, *69*, 83–94. https://doi.org/10.1016/j.tifs.2017.08.018
48. Mantihal, S.; Prakash, S.; Bhandari B. Texture-modified 3D printed dark chocolate: Sensory evaluation and consumer perception study. *J Texture Stud.* **2019**, *50*, 386–399. https://doi.org/10.1111/jtxs.12472
49. Pérez-Monterroza, E.J.; Chaux-Gutiérrez, A.M.; de Moura, M.R.; Aouada, F.A. Fundamentals and functional applications of 3D and 4D printing in food manufacturing. *Processes* **2025**, *13(12)*, 4043. https://doi.org/10.3390/pr13124043
50. Chen, X.; Zhang, M.; Tang, T. Microwave-induced rapid shape change of 4D printed vegetable-based food. *Foods* **2023**, *12*, 2158. https://doi.org/10.3390/foods12112158
51. He, C.; Zhang, M.; Fang, Z. 3D printing of food: pretreatment and post-treatment of materials. *Crit. Rev. Food Sci. Nutr.* **2020**, *60(14)*, 2379–2392. https://doi.org/10.1080/10408398.2019.1641065
52. Soni, R.; Ponappa, K.; Tandon, P. Advancing sustainable food layered manufacturing through 3D printing and post-processing of butterfly pea flower. *Rapid Prototyp. J.* **2026**, *32(1)*, 1–8. https://doi.org/10.1108/RPJ-06-2025-0251
53. Zhou, Q.; Nan, X.; Zhang, S.; Zhang, L.; Chen, J.; Li, J.; Wang, H.; Ruan, Z. Effect of 3D food printing processing on polyphenol system of loaded *Aronia melanocarpa* and post-processing evaluation of 3D printing products. *Foods* **2023**, *12*, 2068. https://doi.org/10.3390/foods12102068
54. Boukid, F.; Hassoun, A.; Zouari, A.; Tülbek, M.Ç.; Mefleh, M.; Aït-Kaddour, A.; Castellari, M. Fermentation for designing innovative plant-based meat and dairy alternatives. *Foods* **2023**, *12(5)*, 1005. https://doi.org/10.3390/foods12051005
55. Lombardi, L.; Gala, L.D.; Esposito, C.; Tammaro, D. Porous architecture in 3D food printing: Advances in formulation, process control, and sustainable structural design. *Compr. Rev. Food Sci. Food Saf.* **2025**, *24(6)*, e70304. https://doi.org/10.1111/1541-4337.70304
56. Zhang, Y.; Raza, A.; Xue, Y.-Q.; Yang, G.; Hayat, U.; Yu, J.; Liu, C.; Wang, H.-J.; Wang, J.-Y. Water-responsive 4D printing based on self-assembly of hydrophobic protein "Zein" for the control of degradation rate and drug release. *Bioact. Mater.* **2023**, *23*, 343-352. https://doi.org/10.1016/j.bioactmat.2022.11.009
57. Lenie, M.D.R.; Ahmadzadeh, S.; Bockstaele, F.V.; Ubeyitogullari, A. Development of a pH-responsive system based on starch and alginate-pectin hydrogels using coaxial 3D food printing. *Food Hydrocoll.* **2024**, *153*, 109989. https://doi.org/10.1016/j.foodhyd.2024.109989
58. Said, N.S.; Olawuyi, I.F.; Lee, W.Y. Pectin hydrogels: gel-forming behaviors, mechanisms, and food applications. *Gels* **2023**, *9(9)*, 732. https://doi.org/10.3390/gels9090732
59. de Farias, B.S.; de Cunha, L.B.; Christ Ribeiro, et al. Designing emulsion gels for 3D food printing: structure, stability, and functional applications. *Surfaces* **2025**, *8(3)*, 64. https://doi.org/10.3390/surfaces8030064

 doi:10.20944/preprints202603.0723.v1

60. Hashemi, B.; Jafarzadeh, S.; Mohammadi, R.; Jafari, S.M. Application of oleogels, hydrogels and bigels as novel structured materials in 3D/4D food printing. *Adv. Colloid Interface Sci.* **2025**, *343*, 103578. https://doi.org/10.1016/j.cis.2025.103578
61. Herdeiro, F.M.; Carvalho, M.O.; Nunes, M.C.; Raymundo, A. Development of healthy snacks incorporating meal from tenebrio molitor and alphitobius diaperinus using 3D printing technology. *Foods* **2024**, *13*, 179. https://doi.org/10.3390/foods13020179
62. Ahmadzadeh, S.; Clary, T.; Rosales, A.; Ubeyitogullari, A. Upcycling imperfect broccoli and carrots into healthy snacks using an innovative 3D food printing approach. *Food Sci. Nutr.* **2023**, *12(1)*, 84-93. https://doi.org/10.1002/fsn3.3820
63. Wang, X.; Zhang, M.; Phuhongsung, P.; Mujumdar, A. Impact of internal structural design on quality and nutritional properties of 3D printed food products during post-printing: A critical review. *Crit. Rev. Food Sci. Nutr*. **2022**, *64(12)*, 3713-3724. https://doi.org/10.1080/10408398.2022.2134979
64. Lorenz, T.; Iskandar, M.M.; Baeghbali, V.; Ngadi, M.O.; Kubow, S. 3D food printing applications related to dysphagia: A narrative review. *Foods* **2022**, *11*, 1789. https://doi.org/10.3390/foods11121789
65. Qiu, L.; Zhang, M.; Bhandari, B.; Chitrakar, B.; Chang, L. Investigation of 3D printing of apple and edible rose blends as a dysphagia food. *Food Hydrocoll.* **2023**, *135*, 108184. https://doi.org/10.1016/j.foodhyd.2022.108184
66. Xu, B.; Wang, X.; Chitrakar, B., et al. Effect of various physical modifications of pea protein isolate (PPI) on 3D printing behavior and dysphagia properties of strawberry-PPI gels. *Food Hydrocoll*. **2025**, *158*, 110498. https://doi.org/10.1016/j.foodhyd.2024.110498
67. Yang, Y.; Yang R.; Fang Y.; Hou, H.; Zhao, L. Interfacial thickness and roughness of sesame oil bodies by pH regulation for 3D printed dysphagia foods: Texture, rheology, and oral tribology. *Food Res. Int.* **2026**, *229*, 118501. https://doi.org/10.1016/j.foodres.2026.118501
68. Villa, C.; Teixeira, C.; Carriço-Sá, B.; Dias, C.; Costa, J.; Mafra, I. Enzymatic hydrolysis as a strategy to reduce allergenicity in sesame (*Sesamum indicum*) proteins. *Innov. Food Sci. Emerg. Technol.* **2025**, *106*, 104284. https://doi.org/10.1016/j.ifset.2025.104284
69. Yang, R.; Cheng, Z.; Zhao, Y.; Song, Y.; Shi, X.; Yu, H.; Zhao, L. Peanut oil body as a food-grade ink for 3D printing: Preparation, characterization and performance. *Food Res. Int.* **2025**, *212*, 116486. https://doi.org/10.1016/j.foodres.2025.116486
70. Chao, E.; Li, J.; Duan, Z.; Fan, L. Bigels as emerging biphasic systems: Properties, applications, and prospects in the food industry. *Food Hydrocoll*. **2024**, *154*, 110089. https://doi.org/10.1016/j.foodhyd.2024.110089
71. Chao, E.; Yu, Q.; Li, J.; Fan, L.; Zhou, Y. Intra-phase reinforcement of chitin nanocrystals in bicontinuous bigels: a strategy for high-precision 3D food printing. *Carbohydr. Polym*. **2026**, *379*, 124948. https://doi.org/10.1016/j.carbpol.2026.124948
72. Cen, S.; Meng, Z. Advances of plant-based fat analogs in 3D printing: Manufacturing strategies, printabilities, and food applications. *Food Res. Int*. **2024**, *197*, 115178. https://doi.org/10.1016/j.foodres.2024.115178
73. Cen, S.; Li, S.; Meng, Z. Advances of protein-based emulsion gels as fat analogues: Systematic classification, formation mechanism, and food application. *Food Res. Int*. **2024**, *191*, 114703. https://doi.org/10.1016/j.foodres.2024.114703
74. Liu, X.; Cheng, Y.; Sun, T.; Lu, Y.; Huan, S.; Liu, S.; Li, W.; Li, Z.; Liu, Y.; Rojas, O.J.; McClements, D.J.; Bai, L. Recent advances in plant-based edible emulsion gels for 3D-printed foods. *Annu. Rev. Food Sci. Technol*. **2025**, *16*, 63–79. https://doi.org/10.1146/annurev-food-111523-121736
75. Zhong, Y.; Wang, B.; Lv, W.; Wu, Y.; Lv, Y.; Sheng, S. Recent research and applications in lipid-based food and lipid-incorporated bioink for 3D printing. *Food Chem.* **2024**, *458*, 140294. https://doi.org/10.1016/j.foodchem.2024.140294
76. Johansson, L.; Badager, I.; Krona, A.; Abdollahi, M. Printability and interfacial performance of emulsion gels and bigels in multi-material dual and coaxial food 3D printing. *Food Hydrocoll*. **2026**, *172*, 111964. https://doi.org/10.1016/j.foodhyd.2025.111964

 doi:10.20944/preprints202603.0723.v1

77. Sinha, S.S.; Upadhyay, A.; Singh, A.; Mishra, S.; Pandey, N. Bigels a versatile gel composite for tailored application in food industries: A review. *Food Struct*. **2024**, *41*, 100380. https://doi.org/10.1016/j.foostr.2024.100380
78. Dominguez, R.; Munekata, P.E.S.; Pateiro, M.; Lopez-Fernandez, O.; Lorenzo, J.M. Immobilization of oils using hydrogels as strategy to replace animal fats and improve the healthiness of meat products. *Curr. Opin. Food Sci*. **2021**, *37*, 135–144. https://doi.org/10.1016/j.cofs.2020.10.005
79. Li, X.; Fan, L.; Liu, Y.; Li, J. New insights into food O/W emulsion gels: Strategies of reinforcing mechanical properties and outlook of being applied to food 3D printing. *Crit. Rev. Food Sci. Nutr*. **2023**, *63*, 1564–1586. https://doi.org/10.1080/10408398.2021.1965953
80. Chen, M.; Ma, W.; Yao, S.; Wan, B.; He, Z.; Kong, X.; et al. Morphological modulation of starch chains from nanorod to nanospindle via temperature-controlled rearrangement. *Int. J. Biol. Macromol*. **2025**, *288*, 138670. https://doi.org/10.1016/j.ijbiomac.2024.138670
81. Ruan, S.; Tang, J.; Qin, Y.; Wang, J.; Yan, T.; Zhou, J.; Gao, D. et al. Mechanical force-induced dispersion of starch nanoparticles and nanoemulsion: Size control, dispersion behaviour, and emulsified stability. *Carbohydr. Polym*. **2022**, *275*, 118711. https://doi.org/10.1016/j.carbpol.2021.118711
82. Zhong, Y.; Chen, M.; Yao, S.; Zhu, Q.; Kong, X.; Zhang, H.; Liu, D.; Xu, E. 3D-printable docosahexaenoic acid-rich algal oil emulsion gels functionalized by multi-shaped starch nanorods. *Carbohydr. Polym*. **2026**, *376*, 124840. https://doi.org/10.1016/j.carbpol.2025.124840
83. Li, D.; Yin, H.; Wu, Y.; Feng, W.; Xu, K.-F.; Xiao, H.; Li, C. Ultrastable high internal phase Pickering emulsions: Forming mechanism, processability, and application in 3D printing. *J. Agric. Food Chem*. **2023**, *71*, 18829–18841. https://doi.org/10.1021/acs.jafc.3c05653
84. Li, M.; Feng, L.; Xu, Y.; Nie, M.; Li, D.; Zhou, C.; Dai, Z.; Zhang, Z.; Zhang, M. Rheological property, *β*-carotene stability and 3D printing characteristic of whey protein isolate emulsion gels by adding different polysaccharides. *Food Chem*. **2023**, *414*, 135702. https://doi.org/10.1016/j.foodchem.2023.135702
85. Kuo, Y.-L.; Chou, Y.-J.; Hu, J.-Y.; Ting, Y. Pickering emulsion emulsified using novel cellulose nanofibers significantly lowers the lipid release rate and cellular absorption. *Food Funct*. **2024**, *15*, 4399–4408. https://doi.org/10.1039/d3fo05219b
86. Zhang, M.; Cheng, L.; Hong, Y.; Li, Z.; Li, C.; Ban, X.; Gu, Z. Effects of hydrocolloids on mechanical properties, viscoelastic and microstructural properties of starch-based modeling clay. *Int. J. Biol. Macromol*. **2024**, *266*, 130963. https://doi.org/10.1016/j.ijbiomac.2024.130963
87. Zhang, X.; Liu, Z.; Shi, W. Pickering emulsion stabilized by grass carp myofibrillar protein via one-step: Study on microstructure, processing stability and stabilization mechanism. *Food Chem*. **2024**, *447*, 139014. https://doi.org/10.1016/j.foodchem.2024.139014
88. Li, L.; Geng, M.; Tan, X.; Teng, F.; Li, Y. Insight on the interaction between soybean protein isolate and ionic/non-ionic polysaccharides: Structural analysis, oil-water interface properties investigation and double emulsion formation. *Food Hydrocoll*. **2024**, *150*, 109754. https://doi.org/10.1016/j.foodhyd.2024.109754
89. Li, Y.; Wang, J.; Ying, R.; Huang, M.; Hayat, K. Protein-stabilized Pickering emulsions interacting with inulin, xanthan gum and chitosan: Rheology and 3D printing behaviour. *Carbohydr. Polym*. **2024**, *326*, 121658. https://doi.org/10.1016/j.carbpol.2023.121658
90. An, Z.; Hu, L.; Gong, X.; Wang, W.; Zhang, J.; Mo, H.; Xu, D.; Liu, Z. Exploring mussel adhesive protein as a natural Pickering emulsion stabilizer for 3D food printing applications. *J. Food Eng*. **2026**, *406*, 112811. https://doi.org/10.1016/j.jfoodeng.2025.112811